JET-P(94)19

J G Cordey et al

The Evolution of the Transport through the L-H Transition in JET

JOINT EUROPEAN TORUS

JET-P(94)19

The Evolution of the Transport through the L-H Transition in JET

J G Cordey, D G Muir, V V Parail[1], G Vayakis, S Ali-Arshad, D V Bartlett, D J Campbell, A L Colton, A E Costley, R D Gill, A Loarte, L Porte, A C C Sips, E M Springmann, P M Stubberfield, A Taroni, K Thomsen, M G von Hellermann.

JET Joint Undertaking, Abingdon, Oxon, OX14 3EA, UK.
[1] Permanent address INF Russian Scientific Centre, "Kurchatov Institute", Moscow, Russia.

Preprint of a paper to be submitted for publication in Nuclear Fusion

April 1994

ABSTRACT

The evolution of the energy, momentum and particle transport through the L-H transition are determined in JET NBI heated discharges. Both normal and periodic L-H transitions are studied. It is found that all of the transport coefficients drop at the transition over a wide radial region and not just in the edge region as was previously thought to be the case. Indeed it is shown by two different modelling techniques that the conventional model in which the transport changes in a narrow region at the edge cannot explain the time behaviour of the electron temperature. Measurements of the fluctuation level by reflectometry also show a very fast drop over a wide radial region.

I. INTRODUCTION

The L-H transition has been a subject of intense study since the discovery of the H-mode of confinement some ten years ago [1] and recently the subject has been reviewed comprehensively by Groebner [2]. The conventional view of the events following an L-H transition is that there is an abrupt (~100 μsec) reduction of the transport in a very narrow edge region (~1cm thick) resulting in the formation of what has become known as the transport barrier. The physical background of this model is that the plasma turbulence is localised near rational surfaces and these isolated fluctuations are not linked together in the radial direction. The turbulence is initially damped in the edge region by the shear in the electric field and a transport barrier formed with a width $\Delta r \sim \rho_{\theta i}$, where $\rho_{\theta i}$ is the poloidal ion larmor radius. This is then followed by a reduction in the transport coefficients through the entire plasma on the energy confinement time scale τ_E (~0.5s for JET). We will refer to this model of the transition as the local model.

Recently [3] an analysis of a series of low density high power JET pulses has revealed that the conventional picture does not correctly describe this type of pulse. In particular it has been deduced from the fast response of the electron temperature at the transition [4] that the electron transport must change over a very wide region extending from the edge to a position approximately half way in, in a few msecs (≤4). Similar changes are also seen in the profiles of ion temperature and toroidal rotation at the transition [5] indicating that the ion thermal conductivity and momentum diffusivity also drop abruptly at the transition over a wide radial region. In this paper a more extensive transport analysis of these pulses is completed and comparisons are made with the fluctuation measurements obtained on some of the pulses.

This phenomenon of the fast response of the electron temperature over a wide radial region to the transition is most clearly seen on low density pulses, where the rate of increase of T_e is particularly large. On higher density pulses the effect is still there, but is more difficult to

resolve, except in pulses which exhibit a periodic L-H dither where cross correlation techniques can be used to determine the radial response time. Both the low density single transition pulses and the higher density periodic transition pulses are extensively analysed in the following sections of this paper.

A possible explanation of this phenomenon of the transport changing over a wide region, is that the plasma turbulence is linked in the radial direction by the toroidicity [6]. Analytical estimates [7,8] and numerical analysis [9] show that the characteristic radial correlation length of these structures is of the order of $\Delta r_g \sim \sqrt{a\rho_i}$, where a is the effective minor radius, and ρ_i the ion Larmor radius. This value is an order of magnitude larger than the corresponding value for the local model $\Delta r_l \sim \rho_i$. If the plasma turbulence does form such an extended structure, then the suppression of plasma turbulence in one place (e.g. near separatrix) should lead to the formation of a very wide transport barrier which could be of the order of the plasma minor radius. We will refer to this model of the L-H transition as the global one.

Before proceeding to the discussion of the results we will show the qualitative difference in the dynamics of the L-H transition between the local and global models. Let us assume for simplicity that the electron thermal diffusivity is the only quantity which experiences a change at the time of L-H transition. Assume also that electron temperature reaches its steady state distribution $T_{eo}(\rho)$ before the transition, so that in the L-mode:

$$\frac{3}{2} n_e \frac{\partial T_{eo}}{\partial t} = 0 = \nabla \cdot (n_e \chi_L \nabla T_{eo}) + P(\rho) \qquad (1)$$

where ρ is the effective normalised minor radius which may be expressed via the toroidal magnetic flux Φ: $\pi a^2 \rho^2 B_o = \Phi = \int_S \vec{B} d\vec{s}$, $P(\rho)$ is the input power, and $\chi_L(\rho)$ is the electron L-mode thermal diffusivity. At the start of the L-H transition T_e can be expanded into a steady and time varying perturbation:

$$T_e(\rho,t) = T_{eo}(\rho) + \delta T_e(\rho,t) \qquad (2)$$

where $\frac{\delta T_e}{T_{eo}} << 1$. The evolution of δT_e is described by the following equation

$$\frac{3}{2} n_e \frac{\partial \delta T_e}{\partial t} = \nabla \cdot (n_e \chi_H \nabla \delta T_e) - \nabla \cdot (\chi_L - \chi_H) n_e \nabla T_{eo}. \qquad (3)$$

First, we assume that the local model is valid. In this case $\chi_L - \chi_H$ is non-zero in a narrow region $1-\Delta<\rho<1$, ($\Delta<<1$) near plasma edge only and the second term on the right hand side of Eq.(3) can be interpreted as a heating term localised near the plasma edge. It then follows from Eq. (1) that near the separatrix ($\rho \simeq 1$)

$$\rho n_e \ \chi_L \ \nabla T_{eo} \ (\rho = 1) \simeq -a^2 \int_o^1 P(\rho')\rho' d\rho' \qquad (4)$$

In the limit $\chi_H = \chi_L$ if $\rho \leq 1 - \Delta$ and $\chi_H = 0$ if $1 - \Delta < \rho < 1$

equation (3) can be rewritten in the form,

$$\frac{3}{2} n_e \frac{\partial \delta T_e}{\partial t} = \nabla \cdot \ (\chi_L \ \ n_e \nabla \delta T_e) + \delta(\rho - 1 + \Delta) \frac{a^2}{\rho} \int_o^{1-\Delta} P(\rho')\rho' d\rho' \qquad (5)$$

where $\delta(x)$ is a δ-function.

In the case of a global L-H transition the simplest way to estimate the second term in the right hand side of (3) is to assume that $\chi_H << \chi_L$ everywhere. Together with (1) it leads to the following equation for δT_e:

$$\frac{3}{2} n_e \frac{\partial \delta T_e}{\partial t} = \nabla \cdot \ (n_e \ \chi_H \ \ \nabla \delta T_e) + P(\rho). \qquad (6)$$

By direct comparison of Eqs. (5) and (6), we conclude that the main qualitative difference between the local and global models of the L-H transition is that in the local model the L-H transition is accompanied by the edge localised heating only. In the global model the heating term is distributed over the entire plasma volume (or at least over those parts of plasma volume where $\chi_H \neq \chi_L$). A sketch of the time evolution of the temperature perturbation for the two models is shown in Figs.1a and 1b. It can be seen in both cases that the initial temperature perturbation propagates across the plasma so that after an energy confinement time it is not easy to see the difference between the two models. However with high time resolution ECE electron temperature data the difference between the two models in the early stages can be clearly seen as will be shown in Section IV of this paper.

The structure of the remainder of this paper is as follows: In Section II, a detailed description of the data is given including the various consistency checks that have been made. In Section III a transport analysis is completed through the transition and the reduction in the ion and electron thermal conductivities, the toroidal momentum diffusivity and the particle diffusivity is determined.

Then in Section IV the modelling of the temperature behaviour is discussed using two different techniques. The first technique is a direct simulation technique where a particular model form for the χ_e in L-mode plasmas is reduced first in narrow region at the plasma edge and then over a wider region. It is found that lowering χ_e in the edge region only (the local model) does not

reproduce the correct time behaviour of the temperature in the mid region, whilst the model in which χ_e is reduced over a large radial region (the global model) gives a reasonable fit.

The second method is to model the electron temperature behaviour in the plasma mid region using a heat pulse propagation technique. It is shown that to reproduce the measured ECE temperature behaviour at inner radii one requires a heat pulse χ_{HP} whose magnitude is 10 to 100 times the power balance χ_e and also has a large inward pinch or a χ_e with a very strongly nonlinear dependences on ∇T_e and T_e.

In Section V the fluctuation measurements from reflectometry are presented. Although we were not able to make measurements on all of the pulses in this study, it will be shown that for the periodic L–H dithering pulses there is very sudden drop in the fluctuation amplitude over a region which is similar to the region of improved transport.

Finally in Section VI the results are summarised.

II. DESCRIPTION OF THE DATA

All of the low density pulses used in this paper had an X-point magnetic configuration, a 3 MA current and a toroidal magnetic field between 1.9 and 2.8T. The injection power was in the range between 10 and 16 MW and the target volume average density was ~10^{19} m^{-3}. The Zeff of the target plasma was also low (<2) which is a typical value for low density pulses in a well conditioned machine.

The time development of the energy confinement time, the volume average density, the power, and the D_α trace, are shown in Fig.2 for a typical low field (B=1.9T) pulse. We see that at the transition there is a threefold jump in the confinement. It is this threefold improvement over L-mode which has lead to the term "high performance H-mode" being used to describe these pulses. They are similar to the VH-mode of DIII-D[11], having a large edge bootstrap current and access to a region of second stability against ballooning modes in the edge. There are also similarities with the TFTR supershots in that a necessary condition is low recycling and like supershots they have a peaked density profile.

From Fig. 2 it can be seen that the plasma confinement drops at t=6.3 secs. This loss of confinement is thought to be due to an MHD β limit which restricts the normalised β_N ($\equiv\beta aB/I$) to a value around 2.3. There is some supporting experimental evidence from the magnetic fluctuation measurements for this conjecture. However, as yet, a precise mode identification has not been possible.

In addition to the low density pulses, higher density pulses which have a periodic oscillation ("dither") between the L and H phase[12] with a characteristic frequency in the range 40-75Hz will also be analysed. This behaviour tends to be associated with relatively high edge densities. For these discharges the density at the separatrix was $(1\text{-}1.8)\times10^{19}$ m^{-3}, the central density $(3.5\text{-}4.5)\times10^{19}$ m^{-3} and the volume average density of $(2\text{-}3)\times10^{19}$ m^{-3}. The injection power was relatively low (6-7MW). The typical behaviour of the D_α and average density during a dithering pulse is shown in Fig.3. Following the series of oscillations between the L and H mode, the discharge can be seen to settle into the H-mode at t = 15.1 secs.

We now examine the behaviour of the electron temperature during the transition. For this purpose we use data from the JET Electron Cyclotron Emission diagnostics: the grating polychromator[13] and the heterodyne radiometer[14] both with a time resolution better than 0.5 ms. These two systems are cross-calibrated to the Michelson interferometer[15] on a shot-by-shot basis enabling the simultaneous coverage of a wide radial region in two horizontal planes at 0 and -0.25 m respectively. Fig. 4 shows the ECE temperature at a series of radial positions as a function of time with the D_α signal overlaid. It can be seen that the time delay between the start of the final drop of the D_α signal (the L-H transition) and the response of the temperature, even in the plasma mid region, is very short indeed (~4ms).

Turning now to the ion temperature, T_i, and toroidal angular velocity, Ω_ϕ, which were obtained from the charge exchange recombination diagnostic [16]. These are shown at a series of radial positions versus time in Fig.5. Both measurements show exactly the same feature as the electron temperature measurements, that is, an abrupt change in their rate of increase at the transition right into the plasma mid region (ρ=0.5). The time response of the diagnostic is rather coarse (50msecs), but the effect is very clear.

The electron density also shows a similar behaviour. In Fig.6 the line integrals from the FIR diagnostic [16] are shown for a series of vertical chords through the plasma versus time. These signals are weighted towards the tangency point, and once again there is a fast response to the transition particularly on the outer chords on either side of the centre.

The soft X-ray line integrated emission data, reproduced in Fig.7, also shows a similar response at the transition. The outer and mid channels on either side of the centre respond very quickly to the transition whilst the central channels are unaffected. The soft X-ray data may be used to confirm the electron temperature and Abel inverted density behaviour of Figs.4 and 6. For fixed low z impurity concentration, the line integrals of the soft X-ray emission above an energy threshold imposed by a Be filter may be calculated from the following simple formula.

$$I_x(\rho_T) = A\int_{L(\rho_T)} n_e^2 T_e^{1.3}\, dl \quad ; \quad A = 1{\cdot}14\times10^{-41} . \qquad (7)$$

where ρ_T is the tangency radius, and the units are $I(WM^{-2})$, $n_e(m^{-3})$, $T_e(eV)$, $\ell(m)$.

The simulated line emission and measured line emission are then compared in Fig.8 for three channels, an outer one at R=3.74m, a mid channel at R=3.44m and a central channel at R=3.14m. A good fit to the experimental data is obtained for all three channels, confirming the accuracy of the electron temperature and density profiles.

The transport analysis and modelling described in sections III and IV respectively will be completed mainly using the low field pulse of Figs.4-7, i.e. pulse 26226, since this pulse has the most comprehensive data set. However, there are many other low density pulses in which the fast response to the transition is seen on the temperature data up to the plasma mid region (ρ=0.5). Examples are shown in Figs.9-10. In Fig.9 the electron temperature data for a high field pulse #26061 is shown. This pulse is very similar in character to the lower field pulse 26226, however it has a somewhat cleaner transition as can be seen by comparing the two D_α traces. There is no dither on 26061 prior to the final fall in the D_α trace. The single dither on pulse 26226 is of no consequence in the analysis of Section IV since both modelling techniques use the electron temperature data at an outer radial position as the boundary condition to the analysis, and not a specific time.

In many pulses the transition is triggered by a sawtooth. An example is shown in Fig.10. For this type of transition it is more difficult to determine precisely when the transport changes. However it can be clearly seen that within 10 msecs there is a definite change in the rate of increase of T_e and hence the transport over a wide radial region.

Finally in Fig. 11 the evolution of the electron temperature at several radial positions is shown for one of the periodic L–H dithering pulses, with the D_α trace overlaid. Once again the response of the inner channels is closely correlated with the outer ones. The modelling of this type of pulse is discussed in Section IVc.

III. LOCAL TRANSPORT ANALYSIS THROUGH THE TRANSITION

The FALCON local transport analysis program [17] has been used to follow the evolution of electron and ion heat fluxes, electron density flux and toroidal momentum flux through the L-H transition of pulse 26226 and hence to determine the evolution of the transport coefficients. The errors in the fluxes and transport coefficients can be large because of uncertainties in some of the source terms, e.g. in the electron-ion equipartition term or NBI heating. Since the transition

occurs on a fast time scale and there are no significant changes in the values of temperature or density or rotation velocity (only in their rates of change), these errors can be minimised by taking the difference between the fluxes at time points on either side of the transition and calculating the change in the transport coefficients at the transition. For example, the electron power balance may be expressed in the form:

$$\frac{\partial w_e}{\partial t} = P_\Omega + P_{NBI} + P_{ie} - P_{RAD} - \nabla \cdot q_e \qquad (8)$$

where w_e is the electron thermal energy, P_Ω is ohmic heating, P_{NBI} is neutral beam heating, P_{ie} is equipartition heating by the ions, P_{RAD} is the radiation term, and q_e is the electron heat flux. By taking time points on either side of the transition and sufficiently close to the transition so that the source and sink terms P_Ω, P_{NBI}, P_{ie} and P_{RAD} will not have changed, we can calculate the difference between the fluxes as

$$\left(\frac{\partial w_e}{\partial t}\right)_{t_H} - \left(\frac{\partial w_e}{\partial t}\right)_{t_L} = -\nabla \cdot (q_{eH} - q_{eL}) \,. \qquad (9)$$

where t_L and t_H denote the times immediately before and after the transition.

Assuming the dominant part of the energy flux is conductive, i.e. $q_e = -n_e \chi_e \nabla T_e$, then on integrating Eq. (9), we obtain the change in the electron diffusivity at the transition

$$\Delta\chi_e = \chi_L - \chi_H = \frac{\frac{\partial}{\partial t}\int_o^\rho w_e(t_L) V' \, d\rho - \frac{\partial}{\partial t}\int_o^\rho w_e(t_H) V' \, d\rho}{n_e \nabla T_e} \,.$$

where $V' = dV/d\rho$ and V is the volume enclosed by a flux tube.

Similarly, the changes in the ion thermal diffusivity, χ_i, the toroidal momentum diffusivity, χ_m, and the electron density diffusivity, D_e, can be accurately determined.

Fig.12 shows the evolution of χ_i through the L-H transition of pulse 26226 at four radial positions. There is a clear drop in χ_i at the transition, and the magnitude of the change increases with ρ. Similar features are seen in both χ_e and χ_m and D_e. The change in the diffusivities with radius is shown in Fig.13. With the exception of the particle diffusivity, all have a similar magnitude and similar radial dependencies. There is little change inside ρ=0.3. The change in the particle diffusivity δD_e is smaller than the changes in the other diffusivities but the ratio of the drop to the value in the L-mode is approximately the same for all the diffusivities i.e. $\delta D_e/D_e \sim \delta\chi_e/\chi_e$ etc.

IV. DATA MODELLING

a) Direct modelling using local and global forms of χ_e

In this section, the evolution of the plasma parameters through the transition are calculated for the local and global model forms of χ_e and compared with the measurements. The predictive code JETTO [18] was used. This calculates the electron and ion temperature profile evolution together with the evolution of the electron density and the distribution of the poloidal magnetic fields. However, particular attention was paid to the electron temperature profile evolution because of the availability of the high time resolution T_e data shown in Section II. The following model expression for the electron thermal diffusivity χ_e was used in the numerical analysis:

$$\chi_e = A_1 + A_2 \left| \frac{\nabla n T_e}{n_e} \right| \tag{10}$$

where A_1 and A_2 are numerical parameters, which depend on the transition models (generally speaking they are functions of time and flux coordinate ρ). We deliberately choose the simplest expression for χ_e in order to distinguish the fundamental difference between the local and global models. We do, however, keep the dependence of χ_e on the temperature gradient because such a dependence is usually used to explain the increase of the effective thermal diffusivity observed in almost all experiments on heat pulse propagation. A similar dependence of χ_e on $\nabla n T_e$ was used in [19] to fit the experimentally observed transport in JET L-mode plasma. Three sets of values for the A_1 and A_2 coefficients were used to model L-mode and H-mode phases with the local and global models for χ_e. Two discharges were modelled. The hot-ion H-mode shot #26226 and the periodic dithering L-H pulse #27954.

As was mentioned earlier, the same set of A_1 and A_2 functions was used to describe the L-mode phase of the discharge for both local and global models. To describe the H-mode plasma with the local model of the L-H transition we simply reduce both A_1 and A_2 by a factor of ten near the plasma edge. Due to numerical problems we can not set the width of the transport barrier smaller than $\Delta\rho \approx 0.05$ (which corresponds to $\Delta R \sim 0.05$m). The numerical analysis shows however that the behaviour of the electron temperature far from the transport barrier (for $\rho \leq 0.9$) does not depend on the width of the transport barrier. For the global model of the L-H transition we assume that at the time of the transition the coefficient A_2 is reduced by a factor of ten everywhere. The ρ dependence of χ_e in the L-mode and H-mode for both models is shown in Fig. 14. The actual

reduction coefficients used in numerical simulations were chosen to obtain the best possible agreement with the experimental data.

The characteristic evolution of the electron temperature profile immediately after the L-H transition for the local and global models are shown on Fig. 15. It can be seen that for the local model the electron temperature evolution resembles the usual picture of a heat pulse propagating inwards from the plasma edge. The temperature rises very rapidly near the plasma edge and then the heat wave propagates towards the plasma centre with the a speed which corresponds to an effective thermal diffusivity $\chi_e \simeq \chi_{HP}$. This picture has two peculiarities which make it different from the experimental picture also shown in Fig. 15. First of all the increase of the electron temperature in the inner part of plasma column has a finite time delay which grows toward the plasma centre. And secondly the relative increment of the temperature near the plasma edge is much larger than near the plasma centre. In contrast the global model of the L-H transition leads to a temperature profile evolution which is very similar to the experimental data. This picture leads us to the conclusion that the L-H transition on JET has a global character so that all transport coefficients are reduced at the time of transition not only near the plasma edge but at least everywhere outside the q = 1 surface.

b) Heat Pulse Propagation Method

It was first shown in [3] that the electron temperature behaviour in the plasma mid region could not be described by conventional heat pulse propagation. The change of temperature at the inner radii being too fast for the typical χ_e values derived from power balance studies or from heat pulse propagation. In this section we extend the analysis to determine what forms of χ_e would be needed to explain the time behaviour of the electron temperature data.

The linearised form of the electron energy balance, equation (8), takes the following form for the electron temperature perturbation:

$$\frac{3}{2} n_e \frac{\partial \delta T_e}{\partial t} = \nabla \cdot \left(n_e \chi_e^{HP} \nabla \delta T_e \right) \qquad (11)$$

where $$\chi_e^{HP} = \frac{\partial}{\partial \nabla T_e} \left(\nabla T_e \, \chi_e(\nabla T_e) \right)_{\nabla T_e = \nabla T_{eo}}$$

Assuming that χ_e has the general form:

$$\chi_e = \chi_{eo}\left(\frac{\nabla T_e}{\nabla T_{eo}}\right)^n\left(\frac{T_{eo}}{T_e}\right)^m \qquad (12)$$

where χ_{eo}, ∇T_{eo} and T_{eo} are the steady-state L-mode profiles of the electron conductivity, temperature gradient and temperature respectively, then

$$\chi_e{}^{HP}\nabla\delta T_e = \chi_{eo}(1+n)\nabla\delta T_e - m\,\chi_{eo}\left(\frac{\nabla T_{eo}}{T_{eo}}\right)\delta T_e$$

Therefore, with this general form for χ_e we can model the evolution of δT_e with both a diffusivity term and an inward pinch term, the magnitude of which are controlled by assigning different values to the powers n and m respectively.

Equation (11) was solved numerically, using a fully implicit flux conserving finite difference scheme, as an initial value problem with a time dependent outer boundary condition. The electron temperature measured by the outer channel of the grating polychrometer was used as the outer boundary condition. The inner boundary condition was $\nabla\delta T_e(\rho = 0) = 0$.

We concentrate on the low field pulse 26226, starting the calculation at the peak of the D_α signal and proceeding for a time period of 30 ms, with the electron temperature data at $\rho = 0.75$ as the outer boundary condition. The results are of course independent of the starting time since the calculation depends only on the evolution of the boundary electron temperature and not on the evolution of the D_α, in fact this is a key advantage of this technique.

In Fig.16) the electron temperature data at the radial positions $\rho = 0.60$, 0.65, 0.70 and 0.75 are compared with the results predicted for a variety of different models for χ_e. The traces shown are: a) the observed ECE temperature; b) the predicted temperature assuming n = 0 and m = 0, i.e. using only the L-mode profile of χ_e ($\chi_e(\rho=0.60) \cong 0.4 m^2 s^{-1}$ and $\chi_e(\rho=0.75) \simeq 1.0 m^2 s^{-1}$ c) the prediction assuming n=4, m=2 and d) n=40, m=39. Figure 17) shows the comparison at ρ=0.6 in more detail for these models and additional ones. Only the very extreme models can give a reasonable fit to the data. In addition, a very strong pinch term (~$100 ms^{-1}$) is needed also. A diffusive term alone is not sufficient to drive the large perturbations observed inside the boundary.

Thus, in conclusion, only unrealistic extremely non-linear forms for χ_e as a function of T_e and ∇T_e can account for the fast response of the electron temperature in the plasma mid region ($\rho = 0.5$) to the transition.

c) Modelling of the periodic L-H transitions

To complement the information gathered from observations of heat-pulse propagation, it is possible to observe the effects of the dithering L-H transition as it propagates into the plasma by cross-correlating signals from different ECE channels and recording the phase (time) delay at the frequency of the dither. The results of this procedure are shown in Fig. 18, where the cross-phase between a reference channel (#6) and the rest of the ECE array is plotted against radius. A lower limit on the propagation velocity of ~160m/s can be deduced, indicated by the line through the reference channel.

From the theoretical point of view the main advantage of these L-H oscillating transitions is that they have one main frequency and this allows us to obtain a simple analytical solution. First the problem is simplified by assuming that the electron thermal diffusivity is the only transport coefficient which is changed during the transition. As was discussed in the previous section, if the local model of the L-H transition is valid the periodic L-H transition can be modelled simply by a periodic change of the edge temperature $T_e(\rho = 1) = T_{eo}(\rho = 1) + \Delta T_e(t)$ where $\Delta T_e(t) = \Delta T_e \sin \omega t$. If we assume for simplicity that $\Delta T_e/T_{eo} << 1$ we can express $T_e(\rho, t)$ as in Eq. (2),

$$T_e(\rho,t) \simeq T_{eo}(\rho) + \delta T_e(\rho,t) \tag{13}$$

where $T_{eo}(\rho)$ corresponds to the stationary L-mode T_e before the onset of the periodic transition and $\delta T_e/T_{eo} << 1$ everywhere. If we assume that χ_e depends on ∇T_e and T_e we can expand the electron transport equation in a similar form to Eq. (11)

$$\frac{\partial \delta T_e}{\partial t} = \nabla \cdot \left(\frac{\chi_{eff}}{a} \frac{\partial \delta T_e}{\partial \rho} + u \delta T_e \right) \tag{14}$$

where $\chi_{eff} = \chi_{eo} + \dfrac{\partial \chi_{eo}}{\partial \nabla T_{eo}} \nabla T_{eo}$, $u = \dfrac{\partial \chi_{eo}}{\partial T_{eo}} \nabla T_{eo}$.

First we solve Eq. (14) in the limit $\chi_{eff} \dfrac{\partial \delta T_e}{\partial \rho} >> u \delta T_e$ (i.e. no pinch term). With the boundary condition $\delta T_e(\rho = 1) = \Delta T_e \sin \omega t$, the solution for $\chi_{eff} = \text{const.}$ in slab geometry is:

$$\delta T_e(\rho,t) = \Delta T_e \exp\left(-\sqrt{\frac{\omega a^2}{\chi_{eff}}}(1-\rho) \right) \sin\left(\sqrt{\frac{\omega a^2}{\chi_{eff}}}(1-\rho) + \omega t \right) . \tag{15}$$

It follows from Eq. (15) that the heat pulse which was initiated near the plasma edge propagates towards the plasma centre with a phase velocity $v_{ph} = \sqrt{\omega\chi_{eff}}$.

In the opposite limit $\chi_{eff}\left|\frac{\partial\delta T_e}{\partial\rho}\right| << u|\delta T_e|$, the heat pulse will propagate inward with the characteristic speed $V_{ph}=u$.

For JET typical conditions for dithering shots i.e. pulse 27954, $\omega\simeq 2.5\,10^2 s^{-1}$, we conclude that with the measured minimum $v_{ph}\sim 1.6\times10^2 m\ s^{-1}$, that either $\chi_{eff}>10^2 m^2 s^{-1}$ in the first limit or in the second limit $\frac{\partial\chi_o}{\partial T_o}\nabla T_o > 10^2 m\ s^{-1}$. These equalities reduce to

$$\left|\frac{\nabla T_{eo}}{\chi_{eo}}\frac{\partial\chi_{eo}}{\partial\nabla T_{eo}}\right| \quad , \quad \left|\frac{T_{eo}}{\chi_{eo}}\frac{\partial\chi_{eo}}{\partial T_{eo}}\right| > 10 \tag{16}$$

with $\chi_{eo}\sim 10$ in the plasma edge region. Either of the inequalities of Eq. (16) requires an unrealistically strong dependence of χ_{eo} on T or ∇T.

For the global model of the transition equation (14) should be replaced by:

$$\frac{\partial\delta T_e}{\partial t} = \nabla\cdot\left(\chi_{eff}\frac{\partial\delta T_e}{\partial\rho} + \delta\chi(\rho,t)\nabla T_{eo}\right) \tag{17}$$

where $\delta\chi$ is the global modification of χ_e at the L-H transition. As we have discussed earlier, the second term in right hand side is equivalent to an additional source of heating which is distributed over the plasma volume. It follows directly from (17) that in the global model the heat pulse induced by repetitive L-H transition can propagate towards the plasma centre with an arbitrarily high phase velocity (the upper bound is simply the group velocity of the turbulence which is responsible for anomalous transport).

This conclusion is confirmed by the numerical analysis of the repetitive L-H transition, the results of which are shown in Fig. 19. It can be seen for the local model of the transition that the characteristic heat pulse propagation speed does not exceed 30 – 40 m s^{-1} in spite of having a dependence of χ_e on ∇T_e. Thus for this type of pulse we also conclude that the global model of L-H transition fits the experimental picture much better than the local model.

V. FLUCTUATION MEASUREMENTS

Measurements of fluctuations by E-mode reflectometry on JET, summarised in Costley et al [20], have shown different behaviour in the Ohmic, L-mode and H-mode phases of the discharge. Whereas in the Ohmic and H-mode phases the radial correlation length of the

fluctuations is very short (of order 5mm), in the L-mode the radial correlation length grows with additional heating power, reaching at least 30mm (the limit of radial separation of the cut off layers for the instrument employed) for a beam power of ~15MW. Although no measurements of the single transition were made with the E-mode system, data on the behaviour of the fluctuations during the periodic L-H transitions were available from the 12-channel O-mode reflectometer[21]. This reflectometer is equipped with detectors measuring a combination of the amplitude and phase, $A\cos(\phi)$, of the field reflected from the cutoff layer. This quantity is related in a non-trivial way to density fluctuations near the cutoff[22]. For most discharges, the frequency response of the detectors was limited to 50kHz in order to extend the size of the acquisition window to 81.92ms, or 4-5 cycles of the transition. Data up to 100kHz are available for some pulses, and show no significant difference in the fluctuation levels. The dithering pulses are characterised by density profiles with a plateau region extending to $\rho \sim 0.75$. This confines the reflectometer operation to $\rho > 0.75$.

At the L-H transition, signalled by the characteristic sharp drop in D_α radiation, the fluctuation power decreases abruptly in channels 2 to 5 of the reflectometer, with the sharpest decrease observed in channels 4 and 5, where the drop is approximately a factor of 10 (Fig.20). Drops in fluctuation power as large as a factor of 20 have been observed for some transitions. The timescale of this change is very fast (<0.2ms) and is coincident to ~0.3ms with the drop in radiation observed by the D_α monitor. Following the initial drop, ELM precursors can appear, causing the partial recovery of the fluctuation power. In the cases where distinct ELMS appear, the fluctuation power can reach L-mode levels before each ELM.

The sharpest drop in the fluctuation power corresponds to the region of the profile where the density gradient is high. For example, for the discharge of Fig.20, no change is seen on channel 6, which is located in the region between the flat central region and the high gradient edge. This may be partly due to the low local density gradient, which will tend to enhance the reflectometer response to smaller radial wave numbers. In discharges with slightly higher density, so that channel 7 at $3 \times 10^{19}/m^3$ is available, channel 6 is transposed to a region of higher density gradient and exhibits a small (3dB) drop. In those cases channel 7 shows no change. This information is summarised in Fig.21, which shows the decrease of fluctuation power as a function of the distance from the sepatrix for five similar shots. The region of significant fluctuation drop has a width of 0.15–0.25m.

From the limits on the timing of the fluctuation level drop between channels 2 and 5 we deduce that the fluctuation level drop propagates inwards (or outwards) with a speed in excess of 150 m s^{-1}. This is in agreement with the propagation of perturbations in the temperature

observed by ECE and analysed in section IV, although the radial extent of observations in that case is slightly larger.

V. CONCLUSION

To summarise it has been shown that in low density pulses the electron temperature over a wide radial region ($0.5<\rho<1$) responds to the L–H transition on a very short time scale (~4ms). This implies that the electron energy transport is changing over a similar radial region in a very short time scale. In particular the time scale for the change in the transport coefficients is much shorter than the plasma profile evolution time which is of the order of 0.5s, the energy confinement time.

Similar large changes over a substantial radial region are seen in the other transport coefficients, χ_i, χ_m and D, however the sampling of the ion temperature data is rather course and hence the time scale of the change in χ_i and χ_m is less certain.

Two different modelling techniques have confirmed that the electron temperature behaviour cannot be explained by a model in which the transport changes initially only in the edge, unless the transport coefficients have a global nature or are extremely non-linear in ∇T_e or T_e.

The higher density periodic L-H transition pulses exhibit exactly the same features, that is the change in transport propagates with a minimum speed of 160 m s^{-1}. To obtain this velocity of propagation using a local model one would once again need transport coefficients which were highly non-linear functions of T or ∇T. In these pulses the amplitude of the fluctuations also falls very quickly indeed (~0.2ms) over a similar size region.

As was mentioned in the introduction one possible explanation for the transport changing rapidly over a large radial region is that the turbulence is linked in the radial direction by the torodicity [6]. There is also other indirect experimental evidence for the existence of these linked turbulent cells, in that larmor radius scaling experiments in L-mode plasmas on both TFTR [28] and JET [24] show a "Bohm type" scaling which only arises when the cell size is independent of the larmor radius.

REFERENCES

[1] Wagner, F., et al., Phys. Rev. Lett. **49** (1982) 1408.

[2] Groebner, R.J., Phys. Fluids B **5**, 2343 (1993).

[3] Neudachin, S.V., Cordey, J.G. and Muir, D.G., 20th EPS Conf. on Controlled Fusion and Plasma Physics, V17C, Part 1 p.83 Lisboa, 1993, submitted to Nuclear Fusion.

[4] Parail, V.V., Cordey, J.G., Springmann, E., and Taroni, A., JET-P(93)87, submitted to Nuclear Fusion.

[5] Cordey, J.G., Muir, D.G., Neudatchin, S.V., Parail, V.V., et al. Workshop on H-mode Confinement, Japan 1993, published in

[6] Connor, J.W., Hastie, R.J., and Taylor J.B., Proc. Roy. Soc. London Ser. A 365, 1 (1979).

[7] Connor, J.W., Taylor, J.B., and Wilson, M.R., Phys. Rev. Letters **70** (1993) 1803.

[8] Romanelli, F., and Zonca, F., 20 EPS Conf. on Controlled Fusion and Plasma Physics, v17C, part IV, page 1383, Lisboa, 1993.

[9] LeBrun, M.J., et al., Phys. Fluids B, 5 (1993) 752.

[10] Costley, A.E., Cripwell, P. and Vayakis G., JET-P(93) 102

[11] Greenfield, G.M., B. Balet, Burrell, K.M., et al., Plasma Physics Controlled Fusion **35** (1993) B263.

[12] Colton, A., and Vayakis, G., Oscillating L-H Mode Transitions in JET, in preparation for PPCF.

[13] Tubbing, B.J.P., et al. Proc. 12th Eur. Conf. on Controlled Fusion Plasma Physics, Budapest 1985 Vol. 9F-1 (1985) p215.

[14] Bartlett, D.V., Costley, A.E., Jones, S.E., Porte, L., Smith, R.J., Zolfaghari, A., In proceedings of the Eighth International Workshop on ECE and ECRH (Gut Ising, Germnay, 1992).

[15] Costley, A.E., Baker, E., Bartlett, D.V., Campbell, D.J., Kiff, M., Neill, G., In Proceedings of the Fourth International Workshop on ECE and ECRH (Frascati, 1984).

[16] Von Hellermann, M.G., and Summers, H.P. Active beams spectroscopy at JET. Atomic and plasma material interaction processes in controlled thermonuclear fusion, Edited by Janev R.K. and Drawin H.W. 1993.

[17] Hamnen, H., Tibone, F., Corrigan, G., et al., JET report R(90)06, 1990.

[18] Cenacchi, G., and Taroni, A., in 8th Europhysics Conf. on Comput. Physics, Eibsee, 1986.

[19] Taroni, A., Erba, M., Springmann, E., and Tibone, F., 20th EPS Conf. on Contr. Fusion and Plasma Physics, v17C, Part I, p.87, Lisboa, 1993.

[20] Costley, A.E., Cripwell, P., and Vayakis, G., JET-P(93) 102.

[21] Costley, A.E., Cripwell, P., Prentice, R. and Sips, A.C.C., Rev. Sci. Instrum. 61 (1990), pp. 2823-2828.

[22] Mazzucatto, E. and Nazilian, R., Phys. Rev. Lett. 71 (1993) p.1840.

[23] Perkins, F.W., Barnes, C.W., Grisham, G.W., et al., Phys. Fluids B **5** (1993).

[24] Christiansen, J.P., Stubberfield, P.M., Cordey, J.G. et al., Nucl. Fusion **3** (1993) 863.

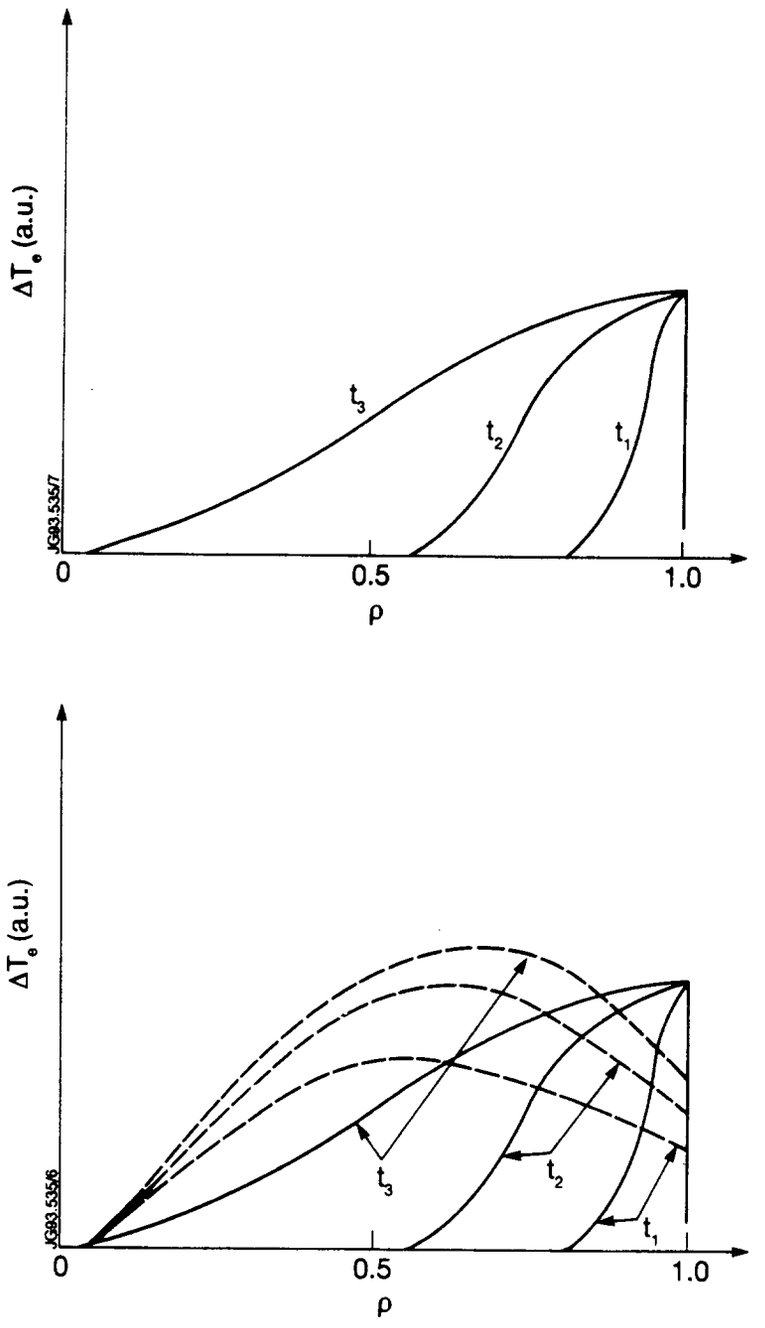

Fig.1. The temporal evolution of the electron temperature perturbation for a) the local model and b) the global model. The dashed line is the contribution from the global change in χ_e and the solid line is the contribution from the change of the boundary condition.

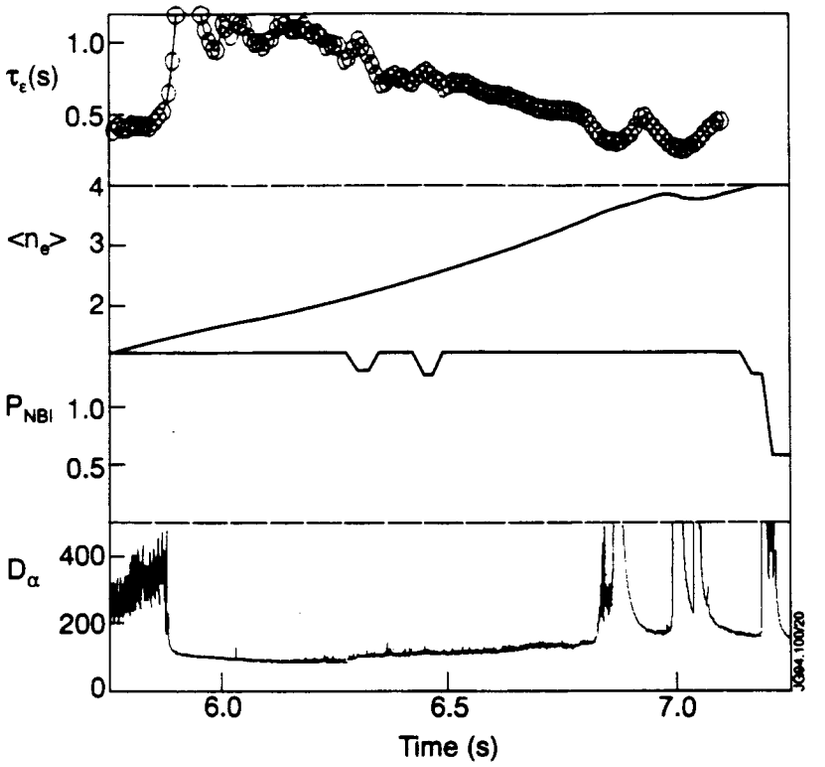

Fig.2. The confinement time, volume average density, NBI power, and the D_α trace versus time for the low field pulse (B=1.9T) #26226.

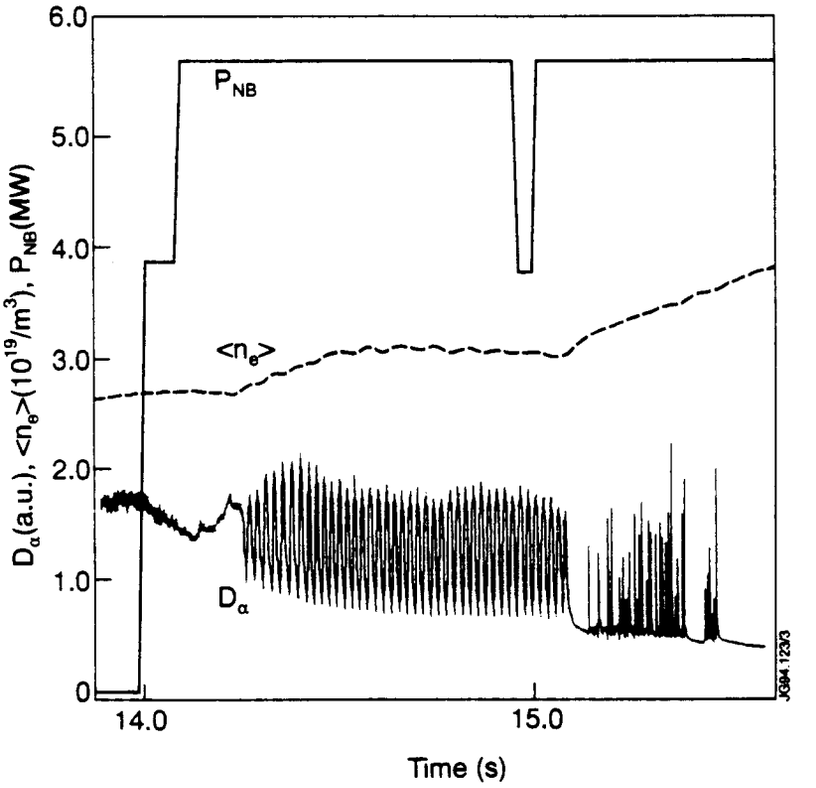

Fig.3. D_α signal, beam power and average density for pulse 24748. A periodic oscillation between the L and H phase with a frequency of ~52Hz can be clearly seen. This is followed by a longer H phase (1s, not shown) terminated when the neutral beam power is abruptly reduced to 1.5MW.

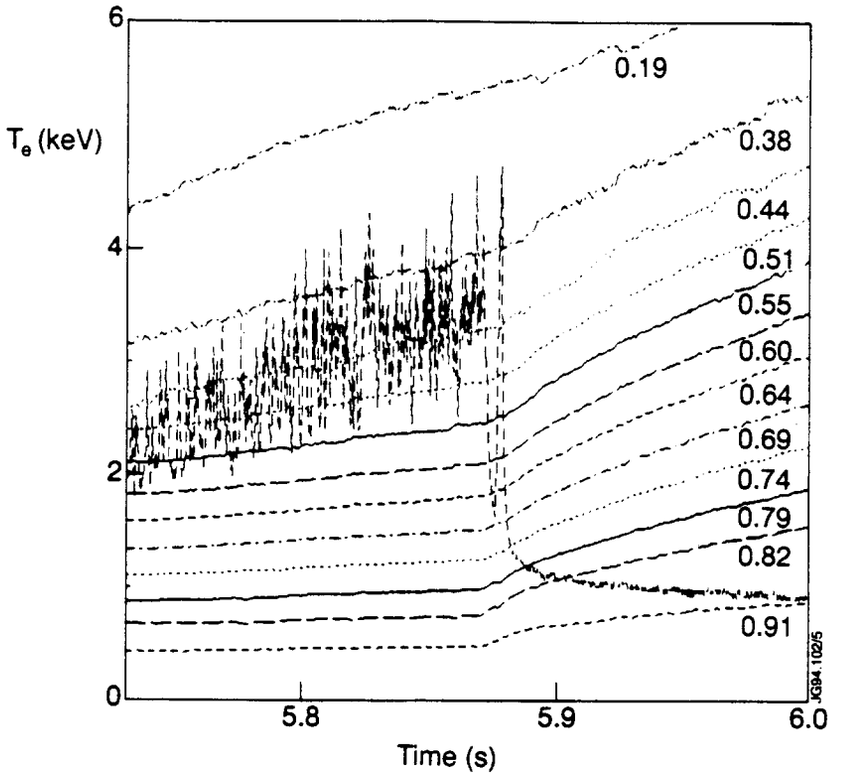

Fig.4. Electron temperature from ECE versus time, for pulse 26226, at a series of radial positions. The data has been smoothed over a 1 msec time interval.

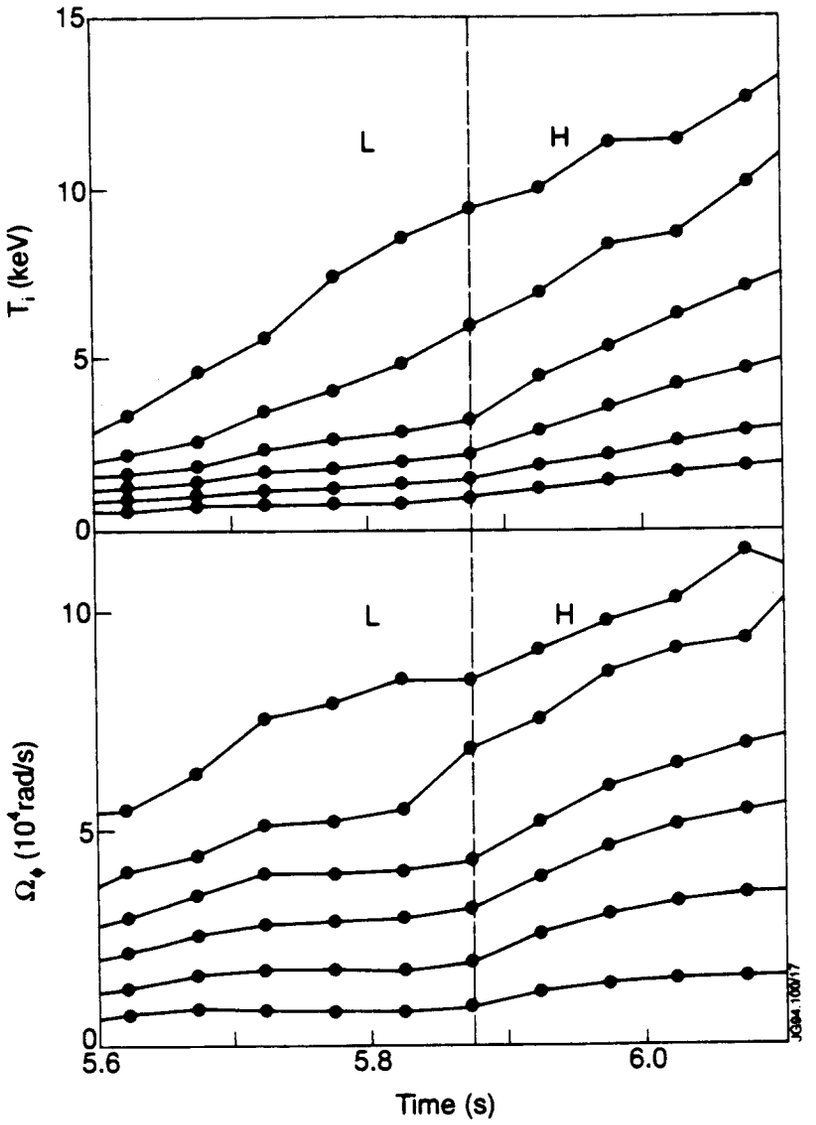

Fig.5. Ion temperature T_i and toroidal angular veloctiy at six radial positions ρ=0, 0.5, 0.6 0.75, 0.9. the dashed line is the start of the final D_α drop.

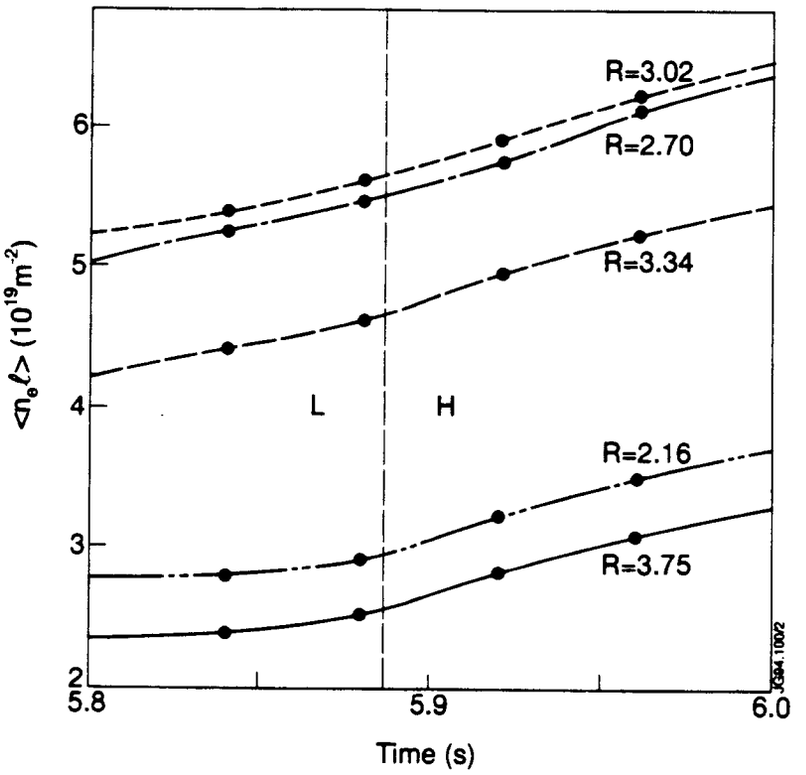

Fig.6. The line integrals of the density from the FIR interferometer.

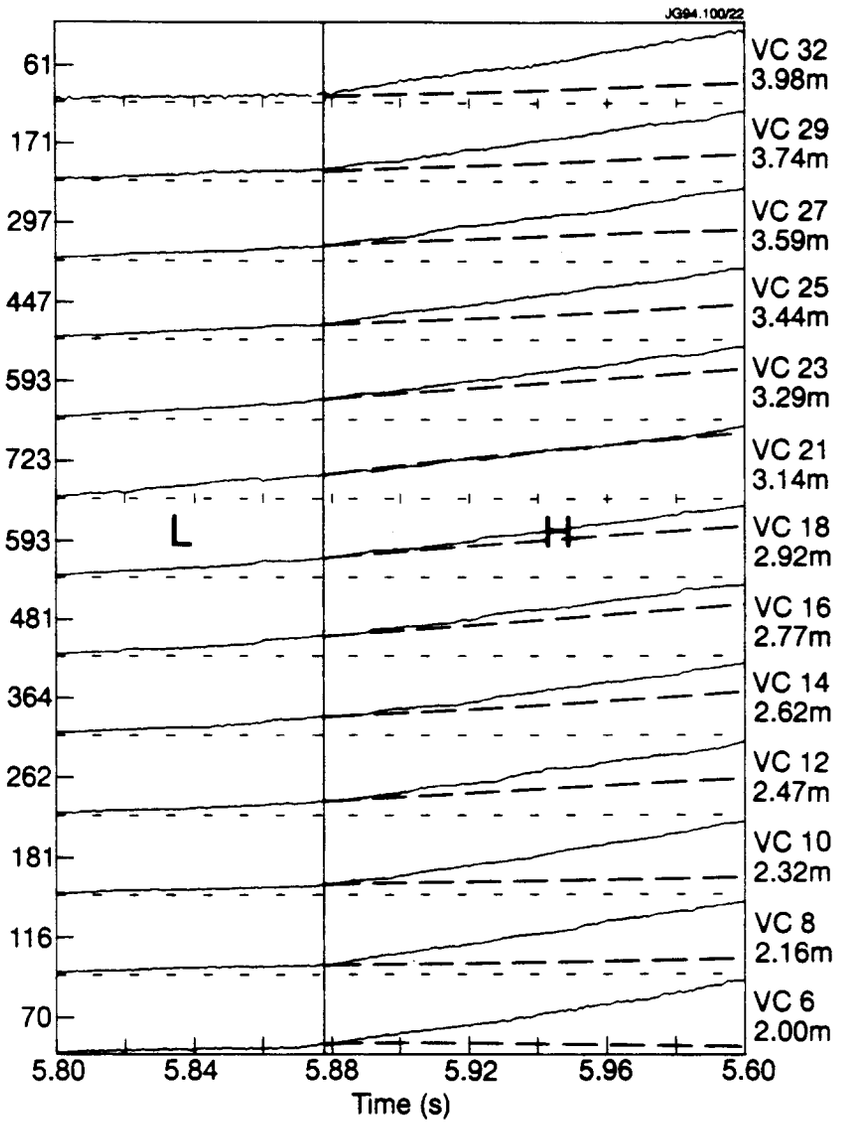

Fig.7. Line integrals of the soft X-ray emission from the vertical camera the R values are the intersections with mid plane.

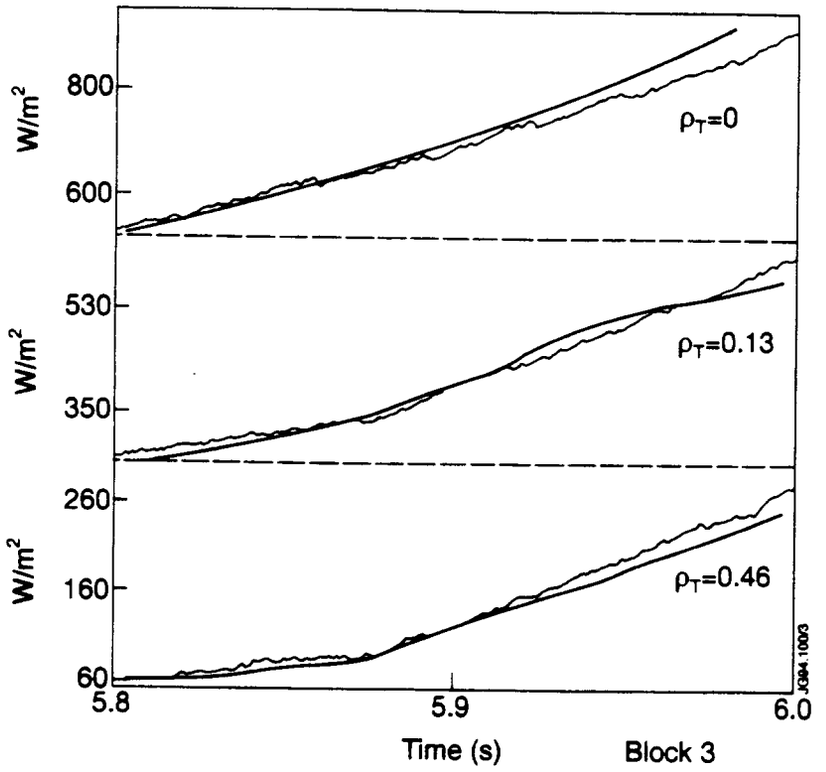

Fig.8. A comparison of three line integrals of the soft X-ray emission from Fig.7 with the simulated data using Eq.7.

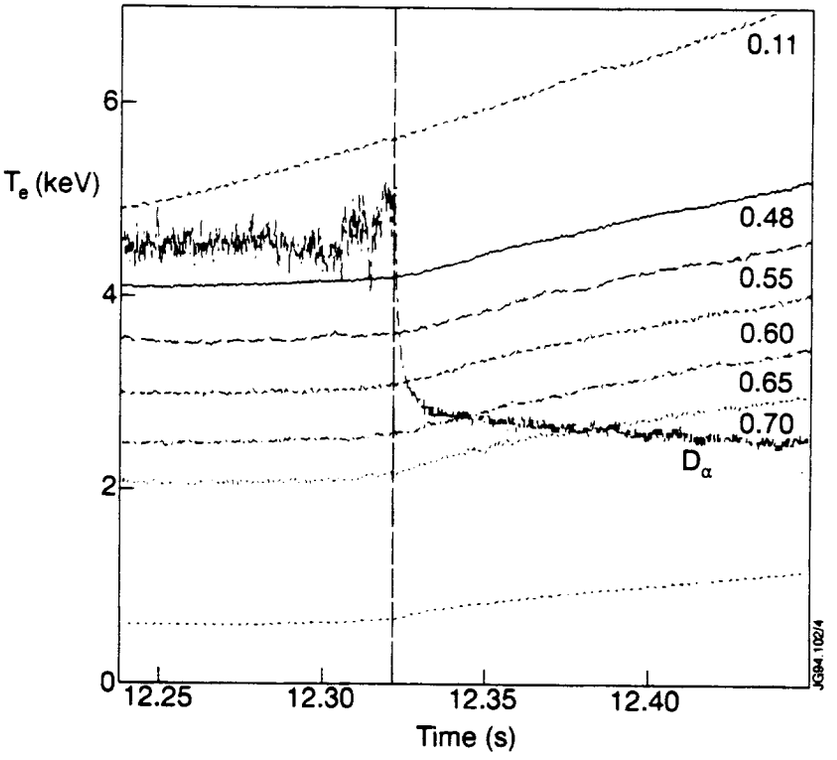

Fig.9. Electron temperature from ECE versus time for pulse 26061 (B=2.87, I=3MA, P_{NBI}=14Mw, target density <n>~$10^{19}m^{-3}$), the D_α trace is overlaid.

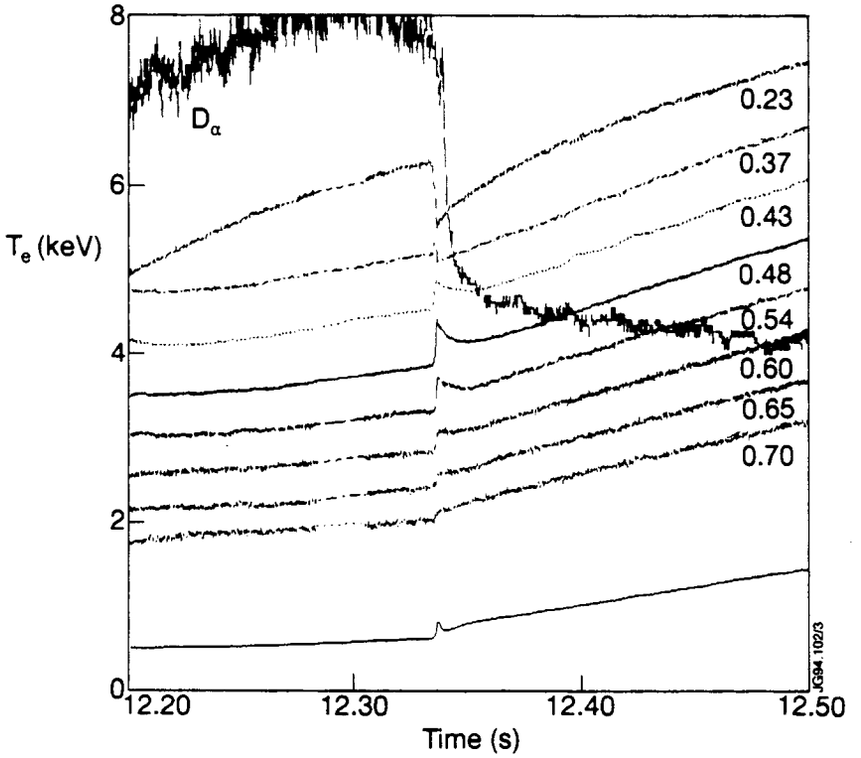

Fig.10. Electron temperature versus time from ECE versus time for pulse 26064 (B=2.87, I=3MA), the transition in this pulse is triggered by a sawtooth. The D_α trace is overlaid.

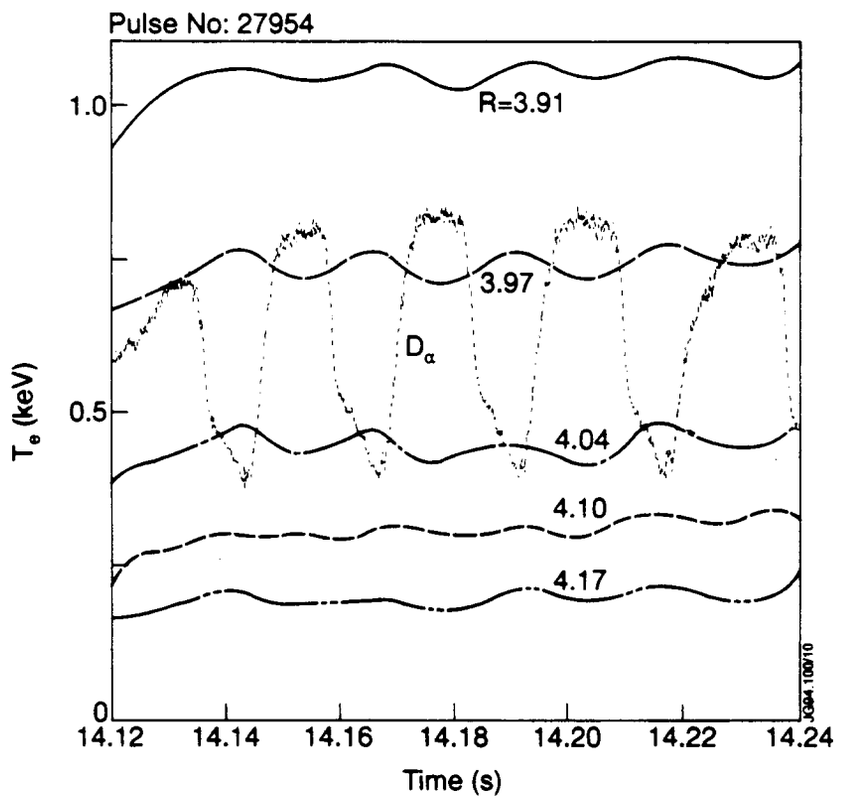

Fig.11. Electron temperature versus time at five radial positions for the periodic dithering L→H pulse 27954 (B=2.8T, I=3MA). The D_α trace is overlaid. The measurement at R=4.17 may be to close to the edge of the plasma for a reliable measurement.

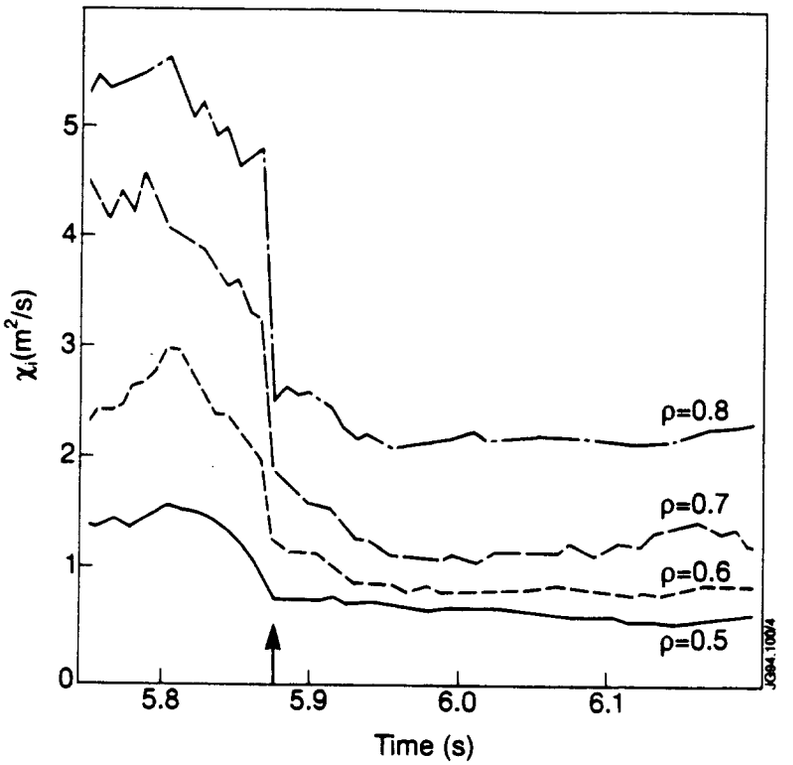

Fig.12. The variation of ion thermal diffusivity χ_i through the transition at four radial positions for pulse 26226. The transition is marked by an arrow.

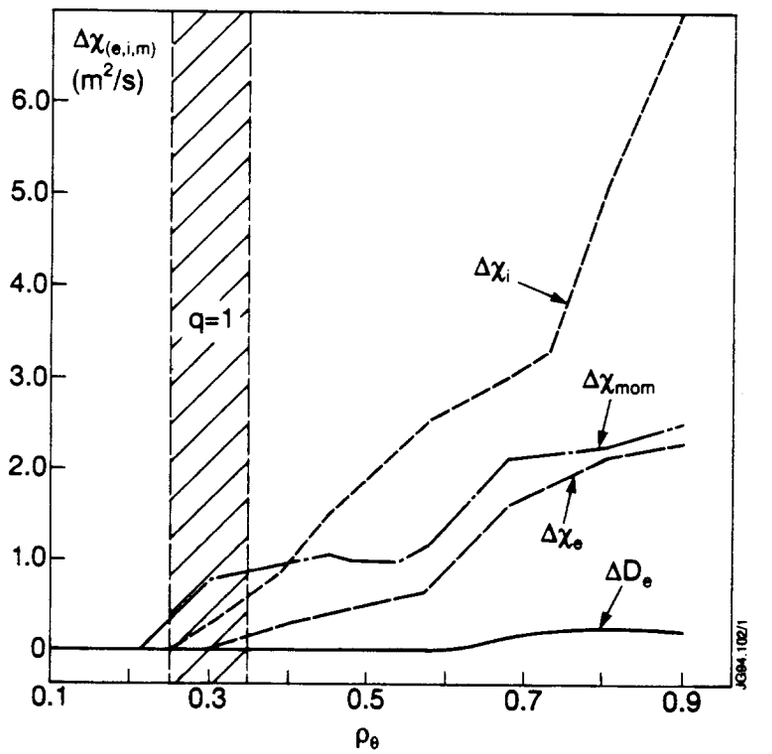

Fig.13. The reduction in the ion thermal diffusivity $\Delta\chi_i$, the toroidal momentum diffusivity $\Delta\chi_m$, the electron diffusivity $\Delta\chi_e$, and the particle diffusivity ΔD_e versus normalised radius ρ.

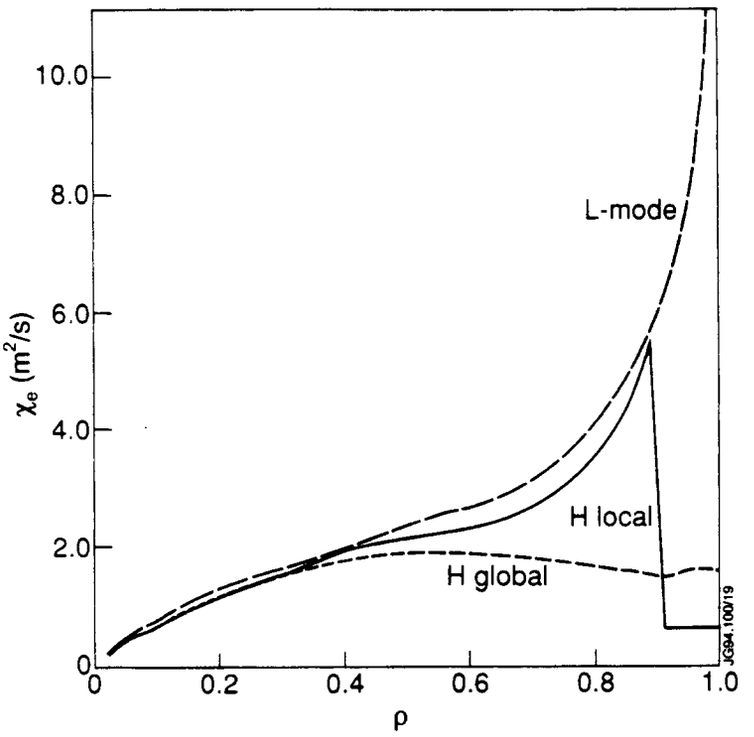

Fig.14. Model forms for the electron thermal diffusivity in L-m ode, and H-mode for the local and global models versus normalised radius ρ.

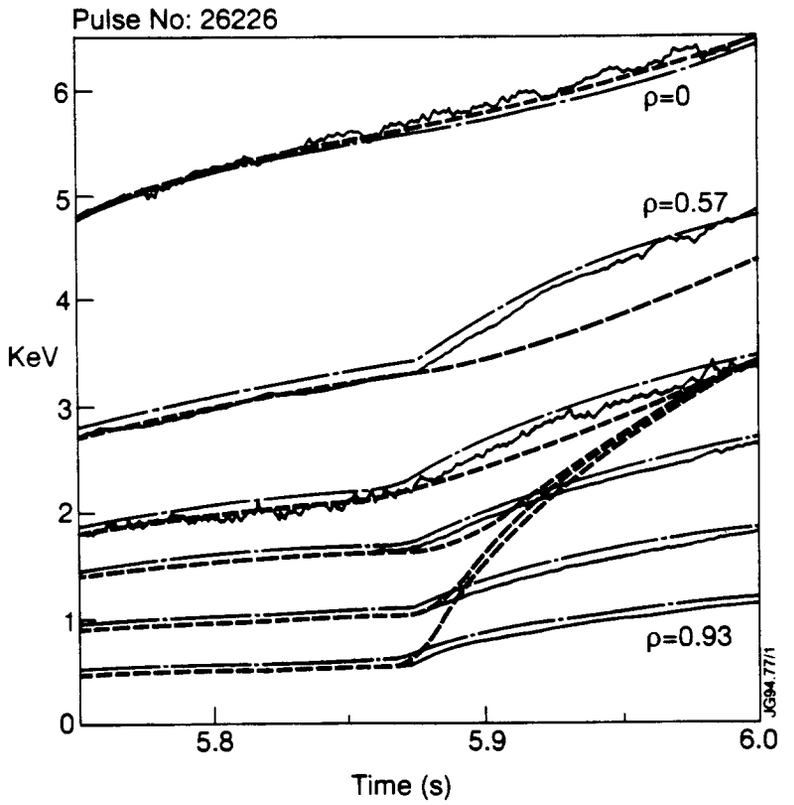

Fig.15. Electron temperature versus time at 6 radial position ρ=0, 0.57, 0.93, the solid curves are the data, the dashed curve is the local model, the dotted is the global model.

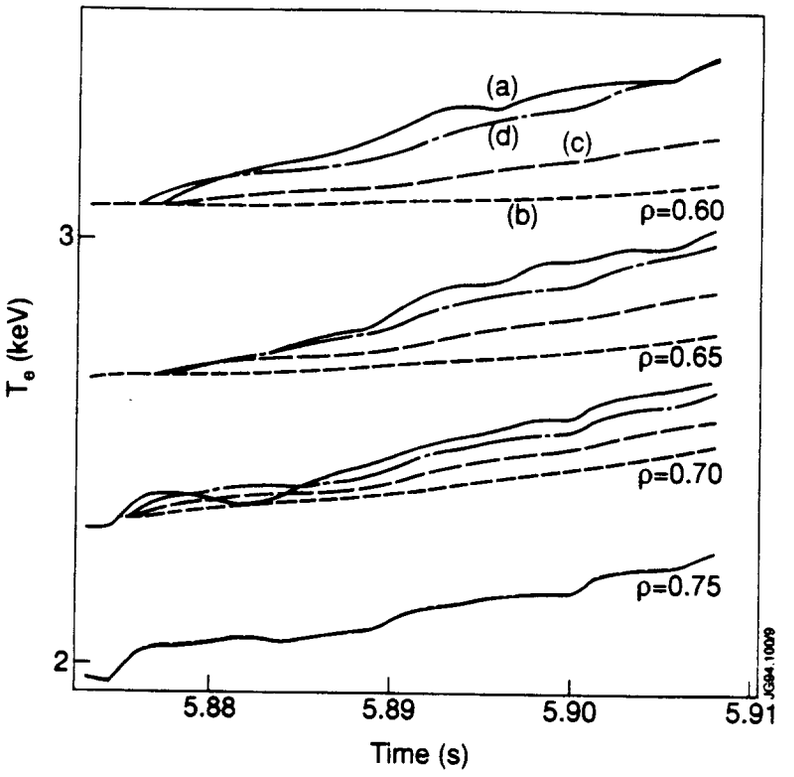

Fig.16. Electron temperature versus time at four radial positions, curves a) ECE experimental data b) the prediction with n=0, m=0, c) n=4, m=2, d) n=40, m=39. n, m are defined in equation (12).

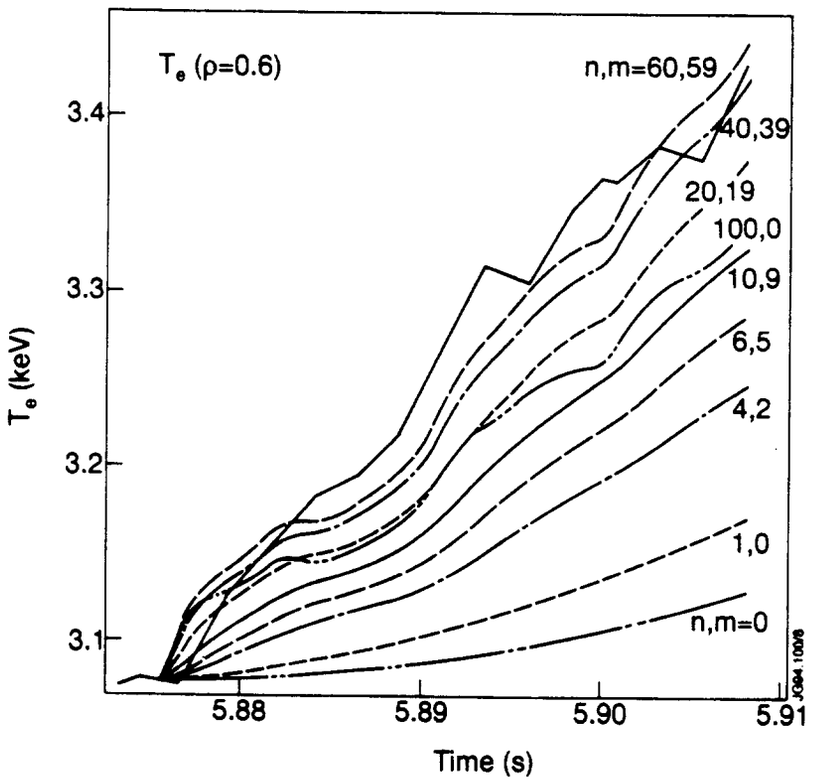

Fig.17. Electron temperature versus time at ρ=0.6. The solid line is the ECE data, the remainder of the lines are predictions for various values of m and n in expression (12).

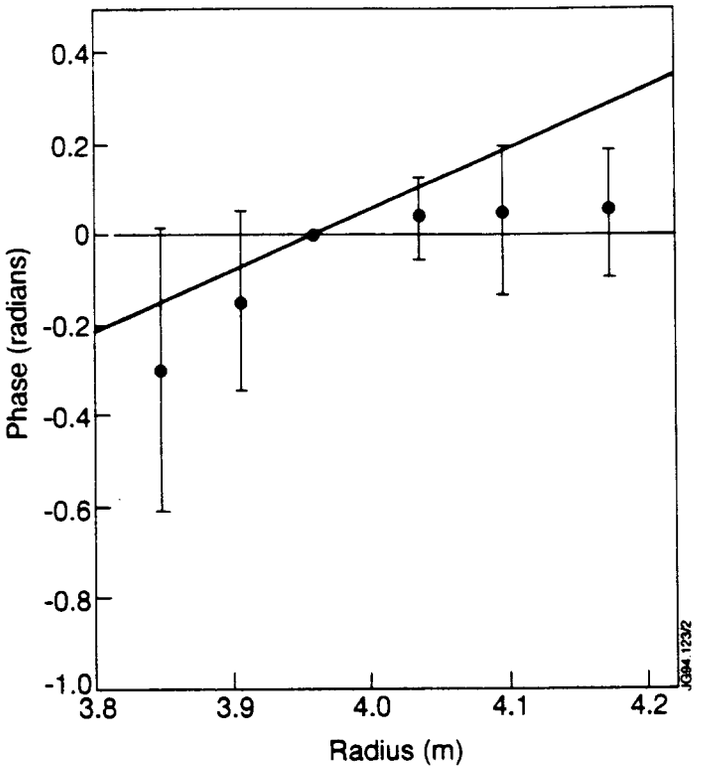

Fig.18. Plot of the phase delay of the temperature fluctuation observed by the ECE grating polychromator with respect to the fluctuation observed on channel 6 (shown with no error bar) for pulse #27954. This is measured at 31Hz, with a bandwidth of 15.5Hz. The line shown corresponds to a phase velocity of 160m/s.

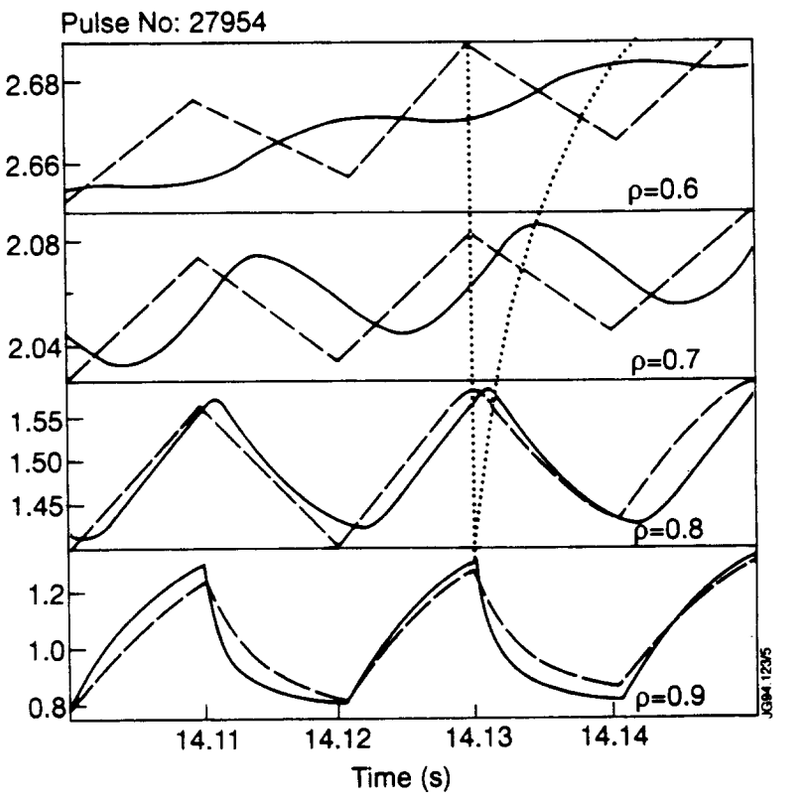

Fig.19. Electron temperature versus time for simulations of pulse 27954. The solid line is for the local model and the dashed line for the global model. The dotted lines connect the peaks of the two models.

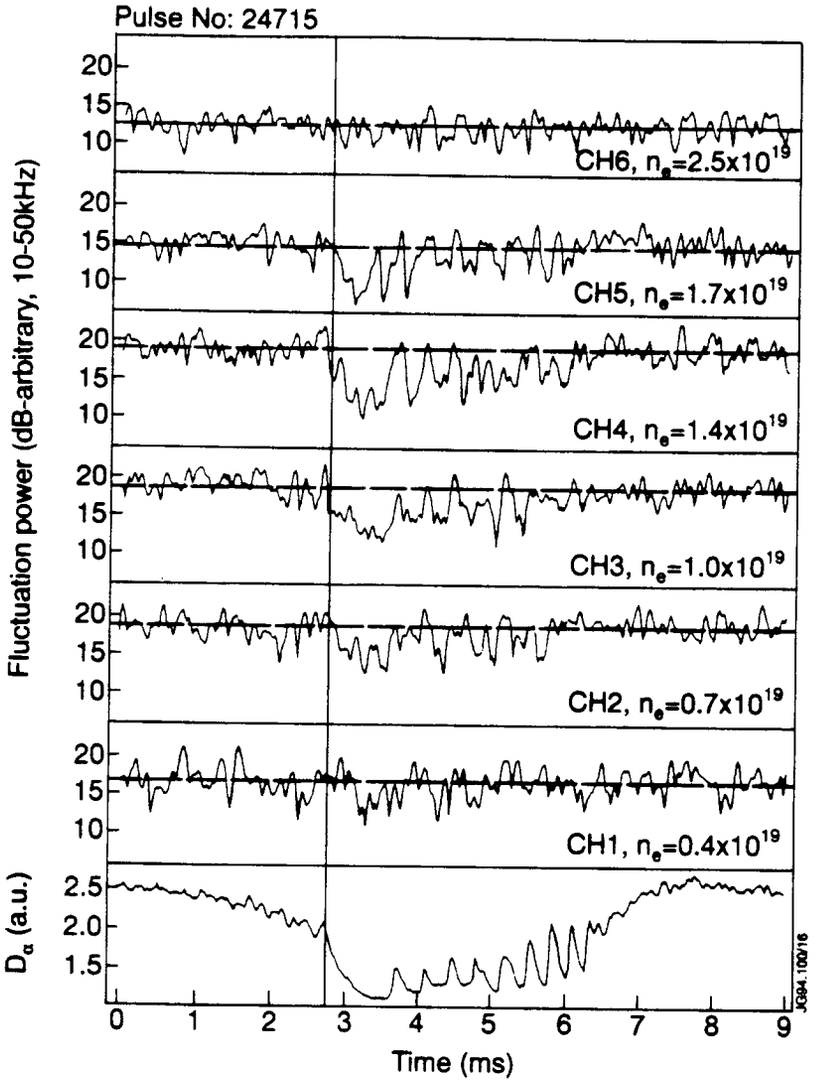

Fig.20. The logarithm of the fluctuation power in the frequency range 10-50kHz for channels 1 through 6 of the O-mode reflectometer, for a typical period of the L-H oscilation ("dither"). ELM precursors can be seen in the H phase of the cycle, particularly on channel 5. The time resolution is 0.1ms.

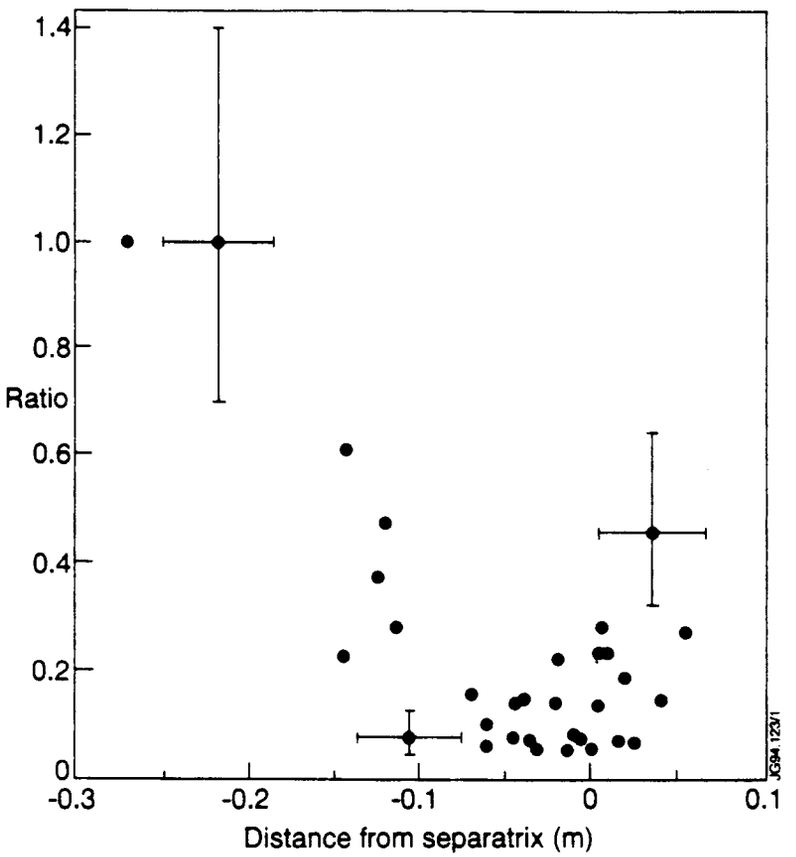

Fig.21. Radial profile of the ratio of the fluctuation power just after the L-H transition to that in the L phase for the same pulse as Fig.20. Results from 5 similar pulses are also shown. Each point is the average of 3 or more cycles of the oscillation.